Characterization of Native Oxide and Passive Film on Austenite/Ferrite Phases of Duplex Stainless Steel Using Synchrotron HAXPEEM

M. Långberg,[1,2] C. Örnek,[1] F. Zhang,[1] J. Cheng,[1] M. Liu,[1] E. Grånäs,[3] C. Wiemann,[4]
A. Gloskovskii,[3] Y. Matveyev,[3] S. Kulkarni,[3] H. Noei,[3] T. F. Keller,[3,5] D. Lindell,[2]
U. Kivisäkk,[6] E. Lundgren,[7] A. Stierle,[3,5] and J. Pan[1,z]

[1]*Department of Chemistry, Division of Surface and Corrosion Science, KTH Royal Institute of Technology, SE-100
44 Stockholm, Sweden*
[2]*SWERIM, SE-16407 Kista, Sweden*
[3]*Deutsches Elektronen-Synchrotron (DESY), 22607 Hamburg, Germany*
[4]*Peter Grünberg Institute (PGI-6), Research Center Jülich, D-52425 Jülich, Germany*
[5]*Physics Department, Universität Hamburg, D-20355 Hamburg, Germany*
[6]*AB Sandvik Materials Technology, SE-81181 Sandviken, Sweden*
[7]*Division of Synchrotron Radiation Research, Lund University, SE-221 00 Lund, Sweden*

A new measurement protocol was used for microscopic chemical analysis of surface oxide films with lateral resolution of 1 μm. The native air-formed oxide and an anodic passive film on austenite and ferrite phases of a 25Cr-7Ni super duplex stainless steel were investigated using synchrotron hard X-ray photoemission electron microscopy (HAXPEEM). Pre-deposited Pt-markers, in combination with electron backscattering diffraction mapping (EBSD), allowed analysis of the native oxide on individual grains of the two phases and the passive film formed on the same area after electrochemical polarization of the sample. The results showed a certain difference in the composition of the surface films between the two phases. For the grains with (001) crystallographic face // sample surface, the native oxide film on the ferrite contained more Cr oxide than the austenite. Anodic polarization up to $1000\ mV_{Ag/AgCl}$ in 1M NaCl solution at room temperature resulted in a growth of the Cr- and Fe-oxides, diminish of Cr-hydroxide, and an increased proportion of Fe^{3+} species.

Many metals spontaneously form oxide films on the surface when exposed to ambient air or aqueous environments. The oxide film is termed as "passive film" if it acts as a barrier against corrosion, i.e., it is able to protect the metal from rapid corrosion. Passive films formed on metals and multi-element alloys, e.g., stainless steels, play a decisive role in their corrosion resistance. The passive films are often a few nanometers thick and composed of oxides and hydroxides of the metal elements. Chemical analysis of the passive films requires surface-sensitive techniques, such as X-ray photoelectron spectroscopy (XPS) or Auger electron spectroscopy (AES).[1,2]

Duplex stainless steels contain approximately equal amount of ferrite and austenite phases in the microstructure, and super duplex stainless steels usually contain high levels of Cr, Ni, Mo and N that give excellent corrosion resistance and mechanical strength of the material. Efforts have been made to analyze the passive films of duplex stainless steels, providing valuable information about the thickness and composition of the passive films formed in different environments.[3–12] It is generally accepted that the passive films are composed of oxy-hydroxides of Fe, Cr and Mo species with some variation in depth. However, due to lack of local chemical information, the difference between the passive films formed on the ferrite and austenite phases is less known. In a few reports, it was claimed that the passive film was homogeneous over the ferrite and austenite phases.[3,4] So far, three different experimental approaches have been reported, aiming to gain local chemical information of the passive films formed on the individual phases: (*i*) local AES analysis in combination with ion sputtering, having a spatial resolution up to 5 μm;[13] (*ii*) selective etching of one of the phases in an acid under potentiostatic control followed by XPS measurement on the remaining phase;[14] and (*iii*) producing the sample material with the chemical composition of the phase of interest, and then analyzing the passive film using XPS.[15]

In the first approach, Auger spectra were collected during local ion sputtering, yielding microscopic elemental information. However, AES does not provide information about oxidation states of the metal elements that are important characteristics of the passive films. The second approach provided information about chemical composition of the surface films on the individual phases, but the etching procedure may cause significant changes (e.g., selective dissolution of certain elements) of the passive films, which are non-uniform for the two phases, so the obtained data do not represent the passive films that are naturally formed on the surface. In the third approach, the passive film of a single-phase microstructure is assumed to have the same composition as the corresponding phase in the duplex-phase microstructure. This assumption is questionable as the chemical composition of the respective phases in the duplex microstructure is highly dependent on the final heat-treatment (solution annealing), which is usually optimized for the specific material. Furthermore, the grain boundaries and residual strains will be different due to different deformation characteristics and thermal expansion coefficients of the two phases, which typically exist in the duplex microstructures.

In this work, we utilized a new method for non-destructive characterization of the passive film of duplex stainless steel using synchrotron hard X-ray photoemission electron microscopy (HAXPEEM), which can access site-specific chemical information with spatial resolution up to 1 μm and depth information between a few to a few tens of nanometres depending on the energy of the beam.[16] By depositing Pt fiducial markers on the sample surface, regions of interest (ROI) can be selected for HAXPEEM measurement and re-measured after ex-situ electrochemical polarization to investigate the difference between the air-formed film and the anodic passive film. Taking an example of a 25Cr-7Ni super duplex stainless steel with typical duplex-phase microstructure, this communication demonstrates the feasibility to characterize the passive films over individual grains of ferrite and austenite phases, and the possibility to re-measure the same sites after ex-situ electrochemical polarization to determine the changes of
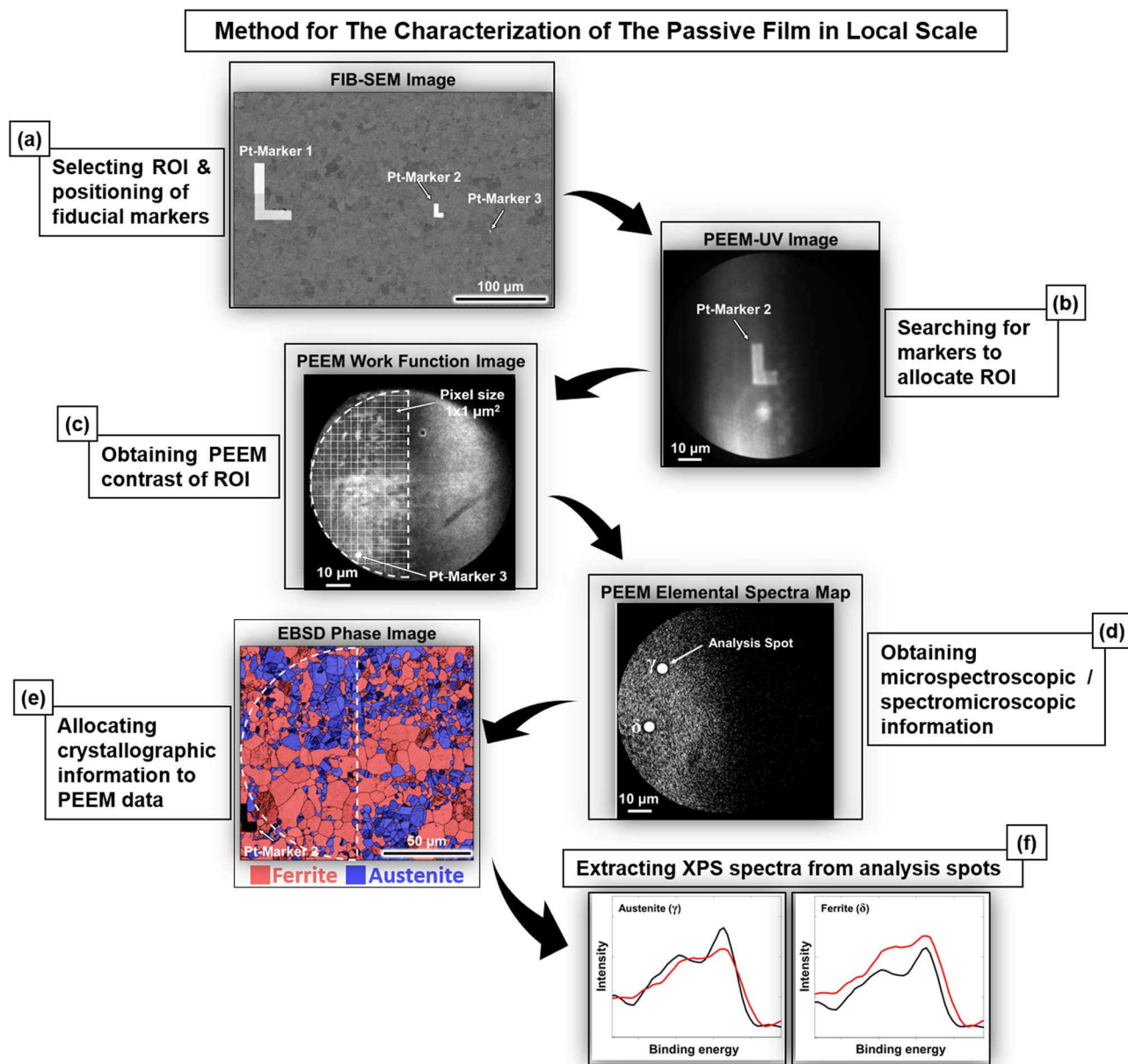
ᶻE-mail: jinshanp@kth.se

Figure 1. Protocol showing the procedure to access local spectroscopic information as an example on duplex stainless steel: (a) Fiducial markers of Pt deposited using FIB-SEM are employed to define the ROI, (b) in UV mode the ROI is located for subsequent PEEM measurement, (c,d) the same ROI is imaged in photoemission mode and a measurement area is defined (half-moon) to collect local (lateral and depth) spectroscopic information with a user-defined pinning of $1\,\mu m \times 1\,\mu m$ size (mesh), (e) the measured ROI can be later re-accessed using EBSD for allocation of crystallographic information (phases, orientation etc.), (f) the spectra obtained can then be associated with the local microstructure as shown by an example on the ferrite and austenite grains with (001) orientation before (native oxide) and after anodic polarization in 1 M NaCl, showing different iron and chromium composition.

the surface oxide film due to anodic polarization, which provides insights into the passivity and passive film of such advanced multiphase alloys.

Experimental

The sample material was grade 25Cr-7Ni super duplex stainless steel (UNS S32750), supplied by Sandvik Materials Technology, Sweden, as plates with 10 mm thickness, which were solution-annealed at 1070°C for 30 minutes. Coupon specimens in sizes of 10 mm × 10 mm × 1 mm were cut along the rolling direction of the plates. The samples were ground down to 4000-grit SiC-sandpaper and then diamond-polished down to $0.25\,\mu m$. Then, the specimens were fine-polished using an oxide-active polishing suspension (OPS, with pH 9–10) to remove surface stresses induced by grinding and polishing. The specimens were re-polished using $0.25\,\mu m$ diamond paste for

1–2 minutes to remove the chemically-altered surface layer due to the OPS polishing. The native surface oxide was formed in ambient air for one week prior to the measurements.

A measurement protocol established at German Electron Synchrotron (DESY, Deutsches Elektronen Synchrotron) was utilized for performing HAXPEEM measurements to extract local surface chemical information from individual ferrite and austenite grains in the duplex microstructure. Using the facilities at DESY NanoLab,[17] the specimens were mounted in a dual beam focused ion beam FIB-SEM instrument to select, image and mark a ROI of ca. $200\,\mu m \times 200\,\mu m$, being representative to the whole microstructure. Pt fiducial markers with $1\,\mu m$ thickness; one large L-shape marker (marker 1) in sizes of $60\,\mu m \times 40\,\mu m$ and another L-shape marker of smaller size (marker 2) in sizes of $20\,\mu m \times 10\,\mu m$ were deposited using ion or electron beam induced local cracking of a Pt containing precursor gas (Figure 1a). In addition, one small marker in sizes of $2\,\mu m \times 1\,\mu m$ (marker 3)

was deposited ca. 50 µm away from marker 2 (Figure 1a). For this smallest, highest hierarchy level marker 3 inside the ROI, electron beam induced deposition was used to avoid beam-induced damage on the oxide/hydroxide and possible ion implantation. As such, the whole ROI including marker 3 could be imaged by HAXPEEM within a field of view of ca. 90 µm × 90 µm and a X-ray beam size of 70 µm × 10 µm. Figure 1a shows an SEM image with all fiducial markers and the ROI. Then, the samples were rinsed with 99% pure acetone, followed by a thorough flush with ultra-pure deionized water and drying by pressurized N_2 streaming gas. The specimens were then transferred to the P22 beamline at PETRA III at DESY for the HAXPEEM measurement. The electrostatic HAXPEEM microscope with an imaging energy filter (NanoESCA, Focus GmbH) was used and operated in collaboration with Forschungszentrum Jülich. The Pt fiducial markers were searched in ultra violet light mode in the ultra-high vacuum (UHV, $1.3 \cdot 10^{-9}$ mbar) chamber at ambient temperature (Figure 1b), and marker 3 was positioned at the left bottom corner of the HAXPEEM image (Figure 1c).

The HAXPEEM measurements were performed at 4 keV, using a raster area of 1 µm × 1 µm, which defines the lateral resolution of the collected spectra. In XPS mode, spectra over a narrow energy range of Fe 2p, Cr 2p, Ni 2p, O 1s, and Mo 3p (near N 1s) were measured consecutively, with an energy resolution of 0.2 eV and 10 sec dwelling time per step. The spectrum of Pt $3d_{5/2}$ was also measured for internal calibration of the energy shift due to electrostatic charge on the sample surface. Then, the sample was taken out from the HAXPEEM chamber, mounted to an electrochemical cell filled with 1M NaCl solution, and polarized at stepwise applied anodic potentials of 600, 900 and 1000 mV vs. Ag/AgCl (sat.) for 10 minutes at each potential. The Pt markers were stable during this electrochemical polarization. This procedure was chosen to reach similar surface condition as reported in earlier work for comparison of the anodic passive film studied with in-situ synchrotron X-ray diffraction measurements.[18] The specimen was then rinsed with deionized water and dried using pressurized nitrogen gas. With the help of the Pt fiducial markers, the same position was found and remeasured with HAXPEEM to analyze the chemical composition of the passive film over the ferrite and austenite formed after the anodic polarization.

Analysis of the XPS spectra was performed after summing up signals originated from a user-defined raster area through pinning of 1 µm × 1 µm size (mesh) over the whole individual grain surface to gain sufficient intensity-to-background signals. Hence, the reported HAXPEEM signals were originated from an area 57 µm² for the austenite and 50 µm² for the ferrite (Figure 1d). The information depth was ca. 18 nm, estimated by 3 times the inelastic mean free path of the emitting electrons.[19] The same ROI was then mapped using electron backscattering diffraction (EBSD) to obtain crystallographic information. Phase maps, showing ferrite in red and austenite in blue, as well as inverse pole figure (IPF) maps normal to sample surface were plotted (Figure 1e). The average grain size of the studied duplex steel was ~20 µm. Only grains larger than ~5 µm in size were chosen to extract local HAXPEEM data (Figure 1f). The XPS spectra were analyzed using CasaXPS V2.3 software. The peak identification and spectra fitting were made after binding energy calibration and Shirley background subtraction with a asymmetric index of 0.1 added to the metallic peaks using Doniach Sunjic line-shape.[20]

Results and Discussion

Only Cr and Fe signals from one ferrite grain and one austenite grain, both with (001) // sample surface, are reported in this communication to show the capability of the method. Extended quantitative analysis of the full data set from the HAXPEEM measurements performed at different X-ray beam energies, including averaging of the grains of each specific phase, will be reported elsewhere.

Figure 2 displays the XPS spectra of Cr and Fe obtained from the ferrite and austenite grains, and the peak assignment as well as the deconvolution of the measured spectra into the metallic, oxide and

hydroxide components. The Cr $2p_{3/2}$ spectra of the native oxide show a metallic peak (Cr^0) with a binding energy at 574.3 eV, an oxide peak (Cr_2O_3) at 576.2 eV, and an increased intensity at higher binding energy that we tentatively assign to a hydroxide peak ($Cr(OH)_3$) at 577.3 eV.[5,14,15] After the anodic polarization, this peak vanished. While the fitting and interpretation of the Cr $2p_{3/2}$ spectra are quite straightforward, it is more complicated for the Fe $2p_{3/2}$ spectra. It is clear that the anodic passive film show more signal at higher binding energy than the native oxide. However, the interpretation of the spectra is not straightforward, since both Fe^{2+} and Fe^{3+} species can be present and the Fe^{2+} species may exist as FeO and Fe_3O_4, while Fe^{3+} species may exist as Fe_2O_3 and FeOOH.[6,14] The quantitative analysis of the Fe-spectra was further complicated by beam fluctuation during the measurements, giving rise to an oscillating background, making it difficult to extract the signal. Though the beam fluctuations were present also for the Cr measurements, the signal was in this case stronger and much easier to extract. For simplicity, we have used three components for fitting the Fe spectra, assigned to Fe^0, Fe^{2+} and Fe^{3+}, and the discussion is focused on the ratio between metallic and oxidative components. The binding energy is 707.2 eV for Fe^0, 708.8 eV for Fe^{2+}, and 711.2 eV for Fe^{3+}, respectively.[5,8] The Fe^{3+} component is not visible in the spectra of the native oxide. Keeping in mind that these spectra were extracted from the PEEM data originated from single grains of several micrometers in size, the relatively low signal intensity and energy resolution do not allow for a more detailed analysis, and this simplified spectra fitting can be regarded as reasonable.

The fitting yielded the atomic percent values of the components for the individual ferrite and austenite grains (Table I). These results, obtained from the same sample surface, enable direct comparison between the ferrite and austenite phases in the duplex microstructure. Based on these data, the ratio between the oxidized and metallic species of Cr and Fe was calculated to access the relative (normalized) amount of the oxide species in the passive film as well as their changes due to the anodic polarization, for the ferrite and austenite grains, respectively. It can be seen from Table I that the air-formed native oxide film on the ferrite seemed to contain more Cr_2O_3 than that on the austenite. Moreover, the oxide/metal ratio indicates a thicker oxide layer for ferrite ($Cr_{ox}/Cr_{me} = 0.93$) than for austentite ($Cr_{ox}/Cr_{me} = 0.65$). Assuming the hydroxide layer was present on top of the oxide layer, the thickness of the oxide layer and hydroxide layer can be calculated based on the intensity of the metallic and oxidative components according to the formula reported in literature,[21] using the electron mean free path at the given photon energy,[22] and the intensity of the metallic and oxidative components. Alternatively, assuming the passive film was a homogeneous layer of oxy-hydroxides of Cr, Fe and Mo, the thickness of the passive film can be calculated following the method reported by Marcus et al.[15] The calculation procedure and results based on the Cr spectra are given in the supplementary material. These calculations are only meant as an example of film characteristics that can be obtained with our approach. A reliable thickness calculation requires higher signal-to-noise ratio for a more reliable spectra de-convolution.

After the anodic polarization, the amount of Cr_2O_3 increased on both phases, indicating a growth of the anodic oxide. $Cr(OH)_3$ became negligible, which was probably due to deprotonation of the hydroxide, since no Cr dissolution from the sample was detected by X-ray fluorescence during the anodic polarization up to 1000 mV/$_{Ag/AgCl}$.[23] The difference in Cr_2O_3 amount in the passive film on the two phases was reduced by the polarization (Table I) The Cr_{ox}/Cr_{me} ratio remained similar for the ferrite (0.93 vs 0.96) and changed from 0.65 to 0.92 for the austenite. The change in the Cr_{ox}/Cr_{me} ratio for the austenite after the anodic polarization suggests a large Cr_2O_3 growth on the austenite, which is absent on the ferrite. These results show that the native oxide films on the ferrite and austenite had different chemical composition and that their change due to anodic polarization was also different.

Regarding the Fe data, it can be seen that the proportion of Fe^0 is similar on the two phases for the native oxide film (Table I). Because
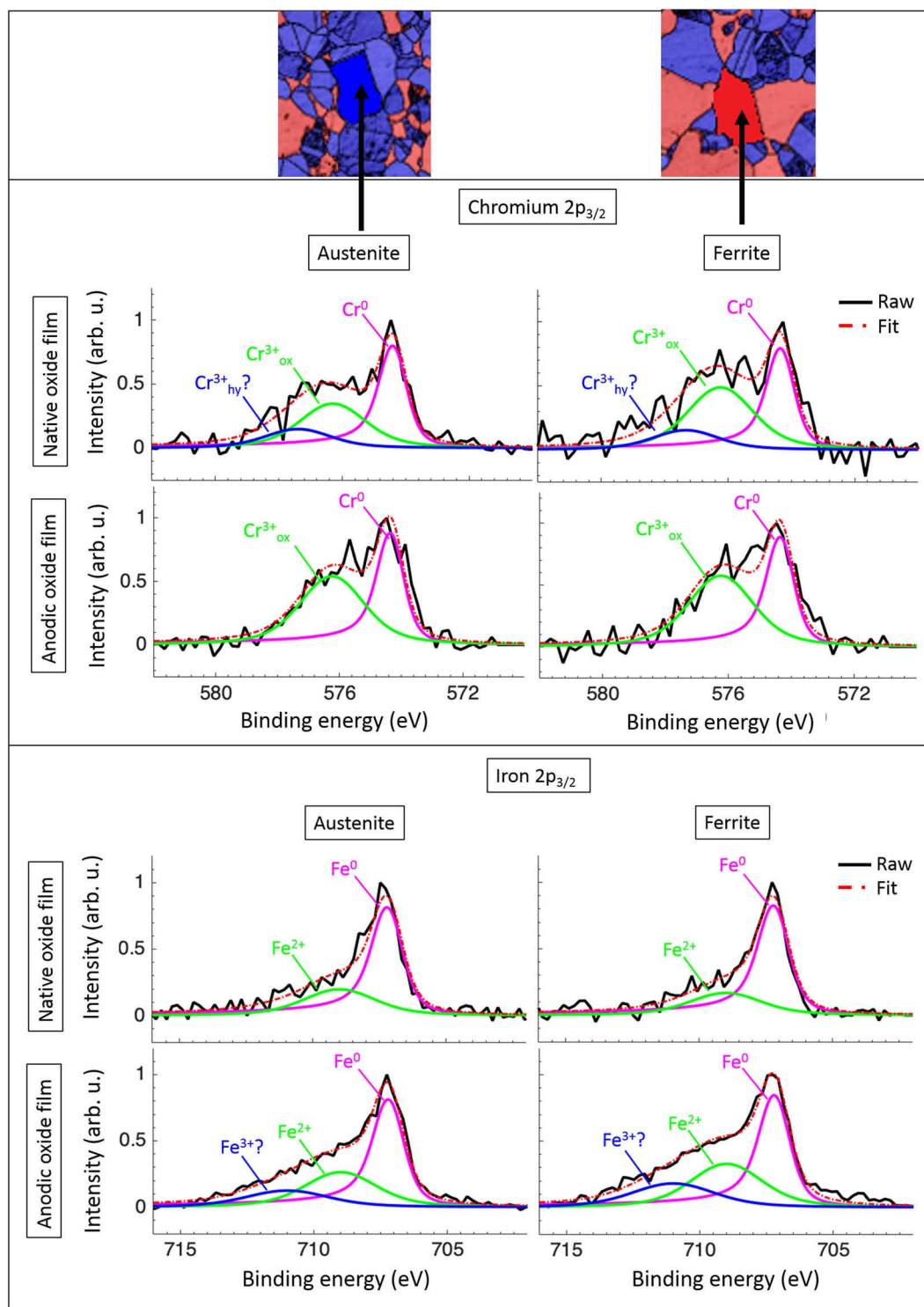
Figure 2. XPS spectra of the peak 2p$_{3/2}$ for Cr and Fe obtained from individual grains (shown in the EBSD graphs on top of the figure) of ferrite and austenite with (001) orientation. The signal shows signs of both metallic and oxidized species. Black curve: native oxide film; gray curve: anodic passive film. Color peaks (deconvoluted components) for Cr^0, Cr$^{3+}_{ox}$, Cr$^{3+}_{hyd}$, Fe^0, Fe^{2+} and Fe^{3+}.

the above-mentioned complications in the quantitative analysis of Fe-spectra, it is hard to ascertain the difference in the Fe-oxides between the two phases (the sum of Fe^{2+} and Fe^{3+} is similar). Nevertheless, certainly there were more Fe-oxides on both phases after the anodic polarization. In particular, the Fe^{3+} species appeared on both phases (Table I). The results suggest that the anodic polarization also caused oxidation of Fe, leading to a growth of Fe-oxides in the passive film with an increased proportion of Fe^{3+} species.

In summary, the results demonstrates the feasibility of the described method for local chemical analysis of the surface oxide films formed on the different phases in the microstructure of the super duplex stainless steel, and the possibility to analyze the same spot before and after electrochemical polarization of the sample. With this method, the local surface analysis can be done without the need for chemical etching or other manipulation of the sample. Using this approach, it is possible to correlate the chemical

Table I. Quantitative XPS analysis of the passive film over austenite and ferrite with (001) orientation before and after the anodic polarization.

Cr components		Cr^0 (at%)	Cr^{3+}_{ox} (at%)	Cr^{3+}_{hyd} (at%)	Cr_{ox}/Cr_{met}
Native	**Austenite**	51	33	16	0.65
	Ferrite	45	42	13	0.93
After anodic polarization	**Austenite**	52	48	~0	0.92
	Ferrite	51	49	~0	0.96

FWHM: 1.04 eV for Cr^0, 2.48 eV for Cr^{3+}_{ox} and Cr^{3+}_{hyd}.

Fe components		Fe^0 (at%)	Fe^{2+} (at%)	Fe^{3+} (at%)
Native	**Austenite**	71	25	~0
	Ferrite	76	22	~0
After anodic polarization	**Austenite**	58	27	15
	Ferrite	52	29	19

FWHM: 1.38 eV for Fe^0, 3.20 eV for Fe^{2+} and 3.70 eV for Fe^{3+}.

information of the passive film as well as its changes caused by the electrochemical reactions (anodic oxide growth and/or dissolution) to the microstructural features, e.g., individual phases or even grains of the duplex stainless steel. Such knowledge will provide a scientific explanation for the experimental observations of the difference in the relative nobility and the selective dissolution of specific phases,[18,23–28] thus contribute to a fundamental understanding of the corrosion mechanism of such alloys. Since advanced multi-components alloys used today possess multi-phase microstructures, this method is valuable in the study of localized corrosion behavior of the alloys.

Conclusions

This work demonstrated the feasibility for microscopic chemical analysis of the surface oxide films formed on polycrystalline multi-phase alloys through HAXPEEM measurements. The following conclusions can be drawn:

• Pre-deposited Pt markers on the sample surface in combination with SEM and EBSD enable HAXPEEM analysis of thin surface films formed on individual grains of the ferrite and austenite phases in the duplex microstructure, and the analysis of the same grain before and after ex-situ electrochemical polarization.

• Direct comparison between the ferrite and austenite phases revealed that certain differences exist in the native oxide film formed on the two phases, and also in the passive film formed after anodic polarization, e.g., the native oxide film on the (001) ferrite grain contained more Cr_2O_3 than that on the (001) austenitic grain; and, anodic polarization up to 1000 mV$_{Ag/AgCl}$ in 1M NaCl solution at room temperature resulted in a growth of the Cr- and Fe-oxides, diminish of Cr hydroxide, and an increased proportion of Fe^{3+} species.

ORCID

M. Långberg https://orcid.org/0000-0001-5207-1132
C. Örnek https://orcid.org/0000-0002-3029-6493
E. Grånäs https://orcid.org/0000-0001-5247-7589
C. Wiemann https://orcid.org/0000-0001-6621-3736
T. F. Keller https://orcid.org/0000-0002-3770-6344
U. Kivisäkk https://orcid.org/0000-0003-3395-7768
E. Lundgren https://orcid.org/0000-0002-3692-6142
A. Stierle https://orcid.org/0000-0002-0303-6282
J. Pan https://orcid.org/0000-0002-4431-0671

References

1. H.-H. Strehblow, *Electrochim. Acta*, **212**, 630 (2016).
2. V. Maurice and P. Marcus, *Prog. Mater. Sci.*, **95**, 132 (2018).
3. C. O. A. Olsson, *Corros. Sci.*, **37**, 467 (1995).
4. C. O. A. Olsson and D. Landolt, *Electrochim. Acta*, **48**, 1093 (2003).
5. C. M. Abreu, M. J. Cristóbal, R. Losada, X. R. Nóvoa, G. Pena, and M. C. Pérez, *Electrochim. Acta*, **49**, 3049, (2004).
6. M. Femenia, J. Pan, and C. Leygraf, *J. Electrochem. Soc.*, **151**, B581 (2004).
7. H. Wang, G. Teeter, and J. Turner, *J. Electrochem. Soc.*, **152**, B99 (2005).
8. Č. Donik, A. Kocijan, J. T. Grant, M. Jenko, A. Drenik, and B. Pihlar, *Corros. Sci.*, **51**, 827 (2009).
9. H. Luo, C. F. Dong, K. Xiao, and X. G. Li, *Appl. Surf. Sci.*, **258**, 631 (2011).
10. H. Luo, C. F. Dong, X. G. Li, and K. Xiao, *Electrochim. Acta*, **64**, 211 (2012).
11. V. Vignal, H. Krawiec, O. Heintz, and D. Mainy, *Corros. Sci.*, **67**, 109, (2013).
12. Z. Cui, L. Wang, H. Ni, W. Hao, C. Man, S. Chen, X. Wang, Z. Liu, and X. Li, *Corros. Sci.*, **118**, 31 (2017).
13. V. Vignal, O. Delrue, O. Heintz, and J. Peultier, *Electrochim. Acta*, **55**, 7118 (2010).
14. Y. Wang, X. Cheng, and X. Li, *Electrochem. Commun.*, **57**, 56 (2015).
15. E. Gardin, S. Zanna, A. Seyeux, A. Allion-Maurer, and P. Marcus, *Corros. Sci.*, **143**, 403, (2018).
16. M. Patt, C. Wiemann, N. Weber, M. Escher, A. Gloskovskii, W. Drube, M. Merkel, and C. M. Schneider, *Rev. Sci. Instrum.*, **85**, 113704 (2014).
17. A. Stierle, T. F. Keller, H. Noei, V. Vonk, and R. Roehlsberger, *J. Large-scale Res. Facilities*, **2**, 1 (2016).
18. C. Örnek, M. Långberg, J. Evertsson, G. Harlow, W. Linpé, L. Rullik, F. Carlà, R. Felici, E. Bettini, U. Kivisäkk, E. Lundgren, and J. Pan, *Corros. Sci.*, **141**, 18 (2018).
19. S. Hofmann, *Quantitative Analysis (Data Evaluation)*, p. 77 in *Auger- and X-Ray photoelectron spectroscopy in materials science: A user-oriented guide*, Springer, Berlin (2013).
20. D. Briggs, *XPS, Basic principles, Spectral Features and Qualitative analysis*, p. 31, in *Surface Analysis by Auger and X-ray Photoelectron Spectroscopy*, D. Briggs and J.T. Grant, Editors., IM publications: Chichester (2003).
21. I. Frateur, J. Lecoeur, S. Zanna, C.-O. A. Olsson, D. Landolt, and P. Marcus, *Electrochim. Acta*, **52**, 7660 (2007).
22. S. Tougaard, *QUASES Software packages to characterize surface nanostructures by analysis of electron spectra*, (http://www.quases.com/), May 2019.
23. M. Långberg, C. Örnek, J. Evertsson, G. S. Harlow, W. Linpé, L. Rullik, F. Carlà, R. Felici, E. Bettini, U. Kivisäkk, E. Lundgren, and J. Pan, *npj Materials Degradation*, **3**, 22 (2019).
24. M. Femenia, J. Pan, C. Leygraf, and P. Luukkonen, *Corros. Sci.*, **43**, 1939 (2001).
25. M. Femenia, J. Pan, and C. Leygraf, *J. Electrochem. Soc.*, **149**, B187 (2002).
26. N. Sathirachinda, R. Gubner, J. Pan, and U. Kivisäkk, *Electrochem. Solid-State Lett.*, **11**, C42 (2008).
27. E. Bettini, U. Kivisäkk, C. Leygraf, and J. Pan, *Electrochim. Acta*, **113**, 280 (2013).
28. C. Örnek, C. Leygraf, and J. Pan, *npj Mater. Degradation*, **3**(1) (2019).